CHAPTER-5

Study of bioactivity of TiO_2 substituted

1393-B3 Borate glass

5.1 Introduction:

In 1969, Prof Hench discovered bioglass, which led to an enormous research interest in the development of bioactive glass materials in the last six decades [1-4]. A bioactive glass material is found to be a great replacement for the bone tissues in our body in case of fractures and other issues. They adopt our body tissue's bond and form a bone shape as required. They are much more adaptable in different sizes as well as in nature [5-7]. They are more efficient than steel as they are inserted in the bone body in fluid forms. The main benefit of these bioactive glasses is their ability to create an amorphous calcium phosphate film. After SBF immersion, the formation of HA was observed [8-9]. Hydroxyapatite (HA –$Ca_{10}(PO_4)_6(OH)_2$), a naturally existing calcium phosphate ceramic, is present in bone and teeth. Metal orthopaedic implants are often coated with HA in order to encourage bone growth around the new implant, but HA is also used in foam and powder forms to help repair bone voids [10-11]. HA is an excellent bioactive, biocompatible compound for regeneration, but poor mechanical properties are its limitations. The occurrence of infections associated with orthopaedic devices is a significant challenge within medical facilities. It may create a loss of bone tissue, several replacement operations, and, in extreme circumstances, amputation infection and even patient death [12]. According to existing literature, the prevalence of infection after implant surgery might reach a maximum of 3%. This rises to 14% in the case of revision procedures [13-14]. The occurrence of osteomyelitis associated with fractures varies depending on the specific bone and kind of fracture. The death rate caused by infection might reach a maximum of 28% [15]. The only possible method of cure in case of such infections is antibiotics. Antibiotics are also harmful to the human body. Bioactive glasses are being used as a substitute material in place of human bone for different applications [16-21]. Bioactive implants are coated with bioactive compounds to decrease the risk of infection

[22]. Titanium dioxide may be subjected to reduction processes to provide a transition metal characterized by relatively low density, and notable strength. Titanium provides a passive TiO_2 layer, allowing improved corrosion resistance [23-25]. Titanium is widely used in the field of bioactive materials [26]. Using titanium alloy, namely titanium oxide, has improved the mechanical strength of materials employed in fracture, spinal fixation and other applications [27-30]. Borate glass was invented by Otto Schott, a German scientist, in the 19^{th} century. Borate glass is a complex composition of silicate glass and alkali ions [31-32]. It is being used in the field of bioactive glass in orthopaedic applications [33-35]. Characterization of titanium ions doping with various components in borate glass was done [36-37]. 1393 glass is widely used in bioactive materials [38-43]. However, the complete replacement of SiO_2 with B_2O_3 causes uncontrollable degradability of the glasses in SBF solution. Such faster degradability is controlled by various researchers [44-45]. 1393-B3 Borate glass with the molecular formula (53-X) B_2O_3, 20CaO, $12K_2O$, $6Na_2O$, 5MgO, $4P_2O_5$ and (X) TiO_2 (wt%) where X = (0.0, 1.0, 1.5, 2.0 and 2.5) are being manufactured. Here, in 1393-B3 glass, silica was replaced with boric oxide to get the result at less melting temperature, resulting in energy saving and more economical bioactive glass. The 1393-B3 glass has shown bioactivity when substituted with various elements [46-47]. Thus, in the present investigation, our aim is to produce bioactive glasses at low temperatures with better mechanical strength and better bone compatibility properties suitable for orthopaedic purposes.

5.2 Materials and methods:

5.2.1 Synthesis of bioglass:

Glass batch calculation is performed to choose the ideal batch of raw ingredients for a glass melt process. All the chemicals are purchased from Loba Chemie Pvt Ltd, which has 98%

purity. To prepare these bio glass samples: boric oxide (H_3BO_3, source of B_2O_3), calcium carbonate ($CaCO_3$ source of CaO), sodium bicarbonate (Na_2CO_3 source of Na_2O), ammonium dihydrogen orthophosphate ($NH_4H_2PO_4$ source of P_2O_5), magnesium carbonate ($MgCO_3$ source of MgO), potassium carbonate (K_2CO_3 source of K_2O) and titanium dioxide (TiO_2) were properly weighed using electronic balance and then mixed in proportion in mortar and pestle as given in Table 5.1. All the chemicals used were of analytical reagent grade, and the weight of various oxides was calculated according to the formula

$$\mathbf{Wa} = \frac{\mathbf{XaZa}}{\sum_{\mathbf{i=1}}^{\mathbf{n}} \mathbf{XiZi}}$$

Wa = Weight fraction, Xa = Mole fraction, Za = Molecular weight of oxide

After preparation, each of the batches was taken in a clean platinum crucible. The crucible was filled with sample batches and placed inside the electric furnace. Each batch is melted at 1100°C for two hours. After homogeneous melting, the glass was poured into a preheated stainless steel plate die, and the obtained sample was placed in an annealing furnace at 500ºC for 2 hours. After 2 hours, the furnace temperature is decreased to room temperature at the rate of 1°C per minute. After the glasses are cooled, they are cut into small pieces, and some glasses are crushed using mortar and pestle and then converted into powdered form with the help of the ball mill technique. Pellets are made from these samples, and their physical, chemical, and mechanical properties like density, compressive strength and flexural strength are measured. SBF is prepared using the well-known Kokubo method [8]. The concentration of SBF closely resembles that of human blood plasma. The samples are kept in small plastic containers in a ratio of 1:100, where 1 is the weight of the sample, and 100 is the weight of the SBF solution in gm [48]. The containers are kept in an incubator at 37°C. The pH value of the samples is measured at intervals of 1,7,15,21, and 28 days. After that, the SBF solution is taken

out from boxes, and it is kept in an air oven at 70°C temperature for drying. Then, these samples are carried to room temperature.

Table 5.1 Composition of BG bioactive glass (wt%).

Chemicals	Base	BG1	BG2	BG3	BG4
B_2O_3	53	52	51.5	51	50.5
CaO	20	20	20	20	20
Na_2O	6	6	6	6	6
P_2O_5	4	4	4	4	4
MgO	5	5	5	5	5
TiO_2	0	1	1.5	2	2.5
K_2O	12	12	12	12	12

5.2.2 Physico-chemical, mechanical and thermal properties:

5.2.2.1 Physico-chemical properties:

Density: Archimedes principle was used to determine the density of the bioactive glass samples taking distilled water as a buoyant material, with an accuracy of 0.001 gm. A digital balance was used to measure all of the weights. According to this principle, the buoyant force acting upward above the axis of the mass of the liquid being moved is equal to the mass of the liquid that the body displaces, whether the body is totally submerged or partly submerged [49].

The density (ρ) of the samples was calculated with the formula:

$$\rho = \frac{w_a}{\omega_a - \omega_b}\rho_b \quad \text{.....(5.1)}$$

Here, ρ_b = Density of buoyant, w_a = Weight of the sample in air, and w_b = Weight of the sample in buoyant

pH measurement: We measured the pH value of the SBF solution after submersing powdered glass samples with the help of the EI Alpha 01 Digital pH Meter at room

temperature for 2, 7, 15, 21 and 28 day intervals, which helped us to analyze the movement of ions in the samples.

5.2.2.2 Mechanical properties:

To measure the mechanical properties, the sample pallets are prepared. Here, the powdered samples are pressed uniaxially at 10-ton pressure in a hydraulic machine for 80 secs. Then, these samples are sintered at 500°C for 2 hrs with a heating and cooling rate of 5° per minute.

Compressive strength: It is also referred to as compression strength, which is the inherent ability of a material or system to resist loads that exert a force aimed at reducing its dimensions [42].

The compressive strength (σ) of the bioactive glass is calculated with the formula:

$$\boldsymbol{\sigma = \frac{F}{\pi r^2}} \quad \text{.....(5.2)}$$

Here, F= load in Newton, r=radius of the pallet

Flexural strength: The flexural strength of a material is often described as the highest amount of bending stress that may be given to the material before it undergoes mechanical deformation [50].

$$\textbf{Flexural strength (MPa)} = \frac{3 \times F \times l}{2 \times b \times h^2} \quad \text{.....(5.3)}$$

Where, F=load in Newton, l=length b=width h =thickness of the pallet

Elastic properties measurement: The velocities of ultrasonic waves, both longitudinal and transverse, were recorded for titanium substituted 1393-B3 borate bioactive glass and the basic glass. These measurements were conducted using the Olympus equipment (M-45, USA) made in the USA. The glass samples, which are to undergo velocity measurements, were

prepared by cutting and polishing them into cubic pieces. The measurement process included determining the time that passed between the commencement of a pulse and the reception of the pulse on the screen of an ultrasonic defect detector. This was achieved using a typical electrical circuit.

Using data on longitudinal and transverse velocities, we calculate the following elastic properties:

1. Poisson's Ratio (υ): It is the deformation of a material perpendicular to the applied load.
2. Young's Modulus (E): It is a material parameter that describes its ability to undergo stretching and deformation.
3. Bulk Modulus (K): It defines the ability of a material to restore its initial volume when subjected to compression.
4. Shear Modulus (G): It determines the level of stiffness exhibited by an object.

We determine these values with the help of the following formulas:

$$\boldsymbol{\nu = \frac{V_L^2 - 2V_T^2}{2(V_L^2 - V_T^2)}} \quad \textbf{.....(5.4)}$$

$$\boldsymbol{E = \frac{\rho V_L^2 (3V_L^2 - 4V_T^2)}{V_L^2 - V_T^2}} \quad \textbf{.....(5.5)}$$

$$\boldsymbol{K = \frac{1}{3}\rho\left(3V_L^2 - 4V_T^2\right)} \quad \textbf{.....(5.6)}$$

$$\boldsymbol{G = \rho V_T^2} \quad \textbf{.....(5.7)}$$

Here, V_T = Transverse velocity, V_L= Longitudinal velocity and ρ=density of the sample.

5.2.2.3 Thermal properties:

Differential scanning calorimetry (DSC) was used to determine the glass transition temperature of experimental compositions and optimal temperatures for isothermal treatments of glasses. Thermo-gravimetric Analysis (TGA) measures the mass of a sample as it is heated, cooled or held at a constant temperature [51]. Here, the heat flow and weight loss value were

measured by heating the borate bioactive samples. The samples were ground in agate mortar with a pestle for 20 minutes before testing. A TG-DSC (Mettler Toledo, Germany) thermal analyzer was used to record DSC and TGA curves in the temperature range from room temperature to 700 ºC with a heating rate of 10°/min.

5.2.3 *In-vitro* analysis:

In-vitro bioactivity studies of the bioglass samples are done after submersing the powdered samples in SBF solution for different time intervals. Then we dried the powdered samples in a hot oven at 70ºC for 48 hours. Other testing techniques, XRD (X-ray diffraction), FTIR (Fourier-transform infrared spectroscopy), and SEM (Scanning electron microscope)/EDAX (Energy dispersive X-ray analysis) results help us to determine the changes in samples after SBF soaking.

5.2.3.1 Phase, functional group and surface morphology study:

Phase analysis, functional group and surface structure study of the bioglass samples are done by using XRD, FTIR and SEM/EDAX techniques. Rigaku Miniflex II XRD machine is used to determine phases of the bioglass samples in the range of 10 to 80º with a scanning speed of 2ɵ using Kα radiations. Bruker Tensor 27 FTIR spectroscope is used to find the functional group present in the samples in the range of 400-4000 cm^{-1}. EVO - Scanning Electron Microscope MA15 / 18 machine gives the surface morphological images of the prepared glass samples to find different elements present in them, and the EDAX part shows the elemental analysis of the sample. All these testing methods show that the HA layer formed on the sample's surface after immersing them in an SBF solution, the composition of which is approximately the same as that of human body plasma.

5.2.4 Hemocompatibility:

Hemolysis occurred tells us its compatibility with human blood. Initially, heparin-coated tubes are used to collect human blood from the median cubital veins, serving as an

anticoagulant. [54-55]. A centrifugation procedure was conducted at a force of 650g for a duration of 10 minutes, with a temperature maintained at 4ºC. After that, the supernatant was properly repudiated. The RBC pellets were cleaned until the supernatant was purified. Subsequently, Phosphate-buffered saline (PBS) was added to dilute the blood in a 1:10 blood-to-PBS ratio. This was followed by adding 0.1 ml of red blood cell suspension (RBCs) and 1 mg/ml (in PBS) of the products to make 0.9 ml. The pH of PBS is 7.4, and it shows no obvious lysis value. Triton X-100 functions as a positive control, signifying complete lysis at a 100% rate. The mixed products were incubated in a shaker-type incubator at 37 ± 1 °C for 1 hour, with constant stirring. Following this incubation period, the mixture was subjected to centrifugation with a force of 650 g for a duration of 10 minutes at 4ºC. This centrifugation stage was performed to separate the non-lysed RBCs from the rest of the components. To evaluate the degree of lysis, the supernatant's optical density at 540nm was evaluated using a microplate reader. The supernatant's optical density at 540nm was evaluated using a microplate reader in order to quantify the degree of lysis [55]. Hemolysis calculated using following equation:

$$\textbf{Hemolysis} = \frac{\textbf{Odsample} - \textbf{Od0}}{\textbf{Od100} - \textbf{Od0}} \textbf{ X 100}$$

Odsample, Od100, and Od0, represented as optical density (OD) values of the samples, positive control (Triton-X) and negative control (PBS), respectively.

5.2.5 *In-vitro* cellular analysis:

The osteosarcoma cell line MG-63 was obtained from NCCS Pune, India. Genetix (Genetix Biotech Asia Pvt. Ltd) were provided DMEM (Dulbecco's Modified Eagle Medium**)** along with a 12-well cell culture plate. From Eppendorf, we bought 96 well plates and T-25 flasks. Gibco supplied us with Penicillin-Streptomycin, FBS (Fetal Bovine Serum) and Trypsin-EDTA. The analysis ingredient from a well-known brand was used to make PBS; for characterization, cell lines were grown in DMEM enriched with 10% FBS and a pen-strep

antibiotic solution. The culture was maintained at a temperature of 37 °C in a humidified atmosphere with 5% carbon dioxide (CO_2). The statistical analysis was performed using one-way ANOVA followed by Tukey's test.

To check cellular compatibility, Cell viability tests were carried out to examine the effect of titanium-substituted borate glass samples (Base, 1%, 1.5%, 2% and 2.5%) on MG-63 cells [54]. 1×10^4 cells were sown in every well of the 96-well cell culture plate and incubated the whole night for adherence. 1 ml of PBS was used to suspend the titanium-substituted borate glass samples at 5 mg/ml stock concentration. The cells underwent treatment with different concentrations (100, 200, 400 and 600 µg/ml) of titanium-substituted borate glass samples and incubated for 24 hours. The exhausted media were discarded, followed by the addition of an MTT-containing medium to each well. The MTT-containing medium was further incubated for 2 hours, and after that, spent media were discarded, and each well received 100 µl of DMSO to dissolve formazan crystal for 30 minutes.

We check the phase images of the samples regularly. The validation of proliferating MG-63 cells was conducted using *in-vitro* live cell pictures using a phase contrast microscope [55]. Following a 24-hour treatment period of samples, pictures were acquired using an inverted phase contrast microscope (EVOS FL cell imaging system, Life Technologies, USA) at 100X magnification.

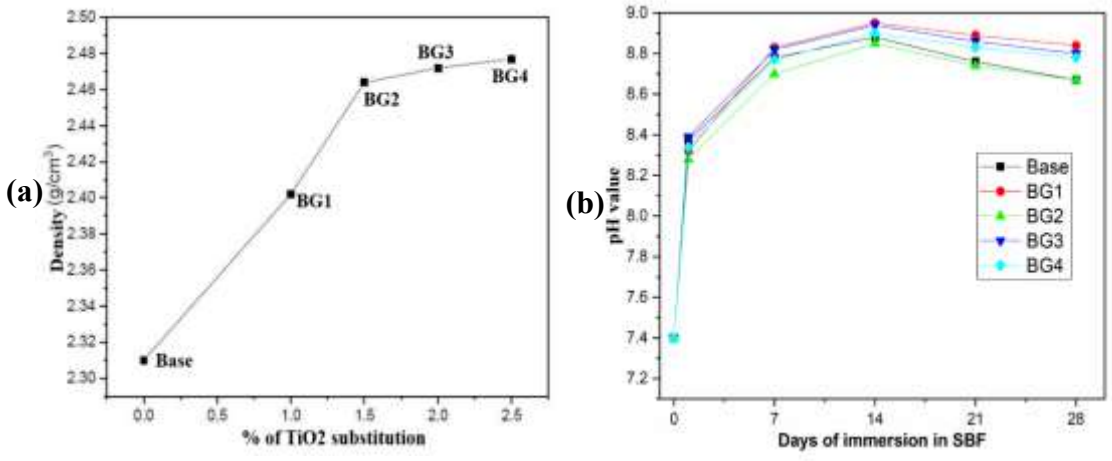

Figure 5.1 (a) Density of base **(b)** pH value, and TiO_2 substituted 1393-B3 glass samples.

5.3 Result and discussion:

5.3.1 Physico-chemical, thermal and mechanical properties:

5.3.1.1 Physico-chemical properties:

Density: The density of the sample is determined by using Equation 5.1. In the 1393-B3 borate glass, Figure 5.1a shows that as the TiO_2 substitution increases, so does the density of the bioactive glass sample. The substitution of B_2O_3 with TiO_2 increases density due to its more precise structural arrangement. Enhancing the compactness of samples contributes to the enhancement of their hardness.

pH analysis: Figure 5.1b depicts the pH fluctuations of the 1393-B3 borate bioactive samples substituted with TiO_2 while submerged in a solution of SBF as a function of the time of immersion. The findings indicated that the pH values of the samples exhibited a rise upon immersion. Indeed, the observed outcome may be attributed to the rise in alkali ions (Na^+, Ca^{2+}, Mg^{2+}) and P^{5+} concentration within the solution, which originates from the dissolving of glass in the SBF solution. This observed fluctuation provides evidence of the ion exchange mechanism occurring between the glass surface and the biological media, potentially promoting the formation of the HA layer [54]. The pH value exhibits an upward trend over a period of 15 days as a result of ion movements facilitating the development of HA. pH value. decline continues until reaching a stable level after a period of 28 days.

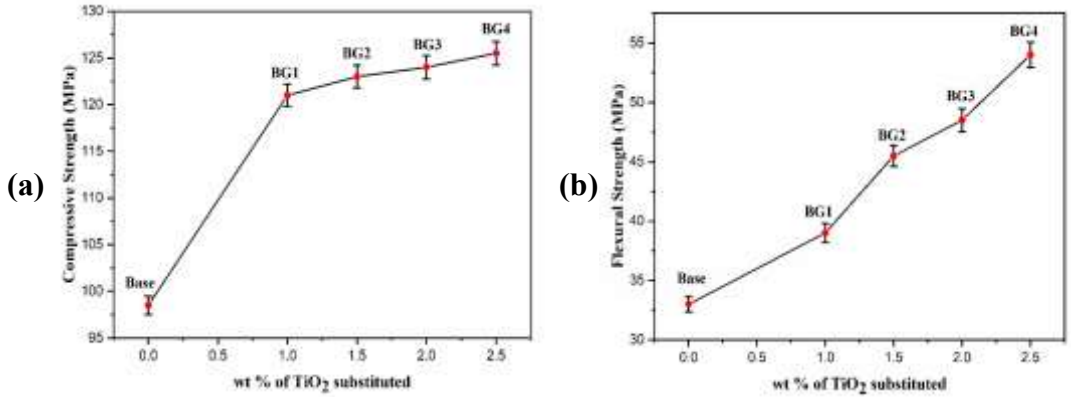

Figure 5.2 Mechanical properties variation of base and TiO_2 substituted 1393-B3 glass samples **(a)** Compressive strength and **(b)** Flexural strength.

Table 5.2 Longitudinal velocity and transverse velocity.

Sample	V_L	V_T
BG0 (1393-B3)	6497	3587
BG1 (TiO_2 1.0%)	6525	3608
BG2 (TiO_2 1.5%)	6566	3641
BG3 (TiO_2 2.0%)	6589	3657
BG4 (TiO_2 2.5%)	6647	3696

Table 5.3 Poisson's ratio, young's modulus, bulk modulus and shear modulus values.

Sample	Y	E	K	G
BG0 (1393-B3)	0.2807	90.022	68.426	35.136
BG1 (TiO_2 1.0%)	0.2797	91.950	69.578	35.915
BG2 (TiO_2 1.5%)	0.2779	94.283	70.764	36.880
BG3 (TiO_2 2.0%)	0.2774	95.705	71.659	37.459
BG4 (TiO_2 2.5%)	0.2762	98.435	73.309	38.563

5.3.1.2 Mechanical Properties:

The compressive strength and flexural strength of the sample are determined by using Equation 5.2 and Equation 5.3, respectively. As shown in Figure 5.2, the sample's flexural and compressive strengths have risen as the TiO_2 substitution increases. The samples exhibit a greater prominence of compressive and flexural strength when subjected to bone contact. Samples of bone tissue linkages grow stronger and more adaptive. It is widely seen that the main drawback of HA lies in its mechanical properties. Even so, through enhanced mechanical properties, these limitations may be effectively reduced.

Elastic properties: The longitudinal velocities and transverse velocities of the bioglass under investigation are shown in Table 5.2. The elastic properties of the BG bioglass samples, Poisson's Ratio, Young's Modulus, Bulk Modulus, and Shear Modulus, are determined using equations 5.4-5.7 respectively. Table 5.3 shows the change in these elastic properties with

different TiO_2 substitution percentages. The analysis of the elastic properties reveals that the substitution of TiO_2 in the 1393-B3 borate glass results in an increase in both longitudinal and transverse velocities, as well as young's modulus, shear modulus and bulk modulus of the bioactive glasses. However, a slight decrease in the value of Poisson's Ratio is observed. The observed increase in the elastic modulus and longitudinal and transverse velocities may be attributed to the concurrent rise in the interconnection of the glass network. The enhancement of the glass network in 1393-B3 borate bioactive glass is seen with increasing TiO_2 substitution. When interatomic distance is considered, the concepts of Young's modulus, bulk modulus, and shear modulus become evident. Specifically, the octahedral coordination of the Titanium ion plays a role in the glass network as modifiers, occupying interstitial positions. This occupation leads to an augmentation in the average quantity of network bonds per unit volume. Therefore, the observed enhancement in these characteristics may be attributed to the contribution of TiO_2, which results in an increase in the interconnectivity within the investigated bioactive glass structure. An increase in the glass network's crosslink density may cause the observed decrease in Poisson's Ratio of the BG bioactive glass sample as the network modifier concentration rises. Crosslink density is defined as the number of bridging bonds per cation.

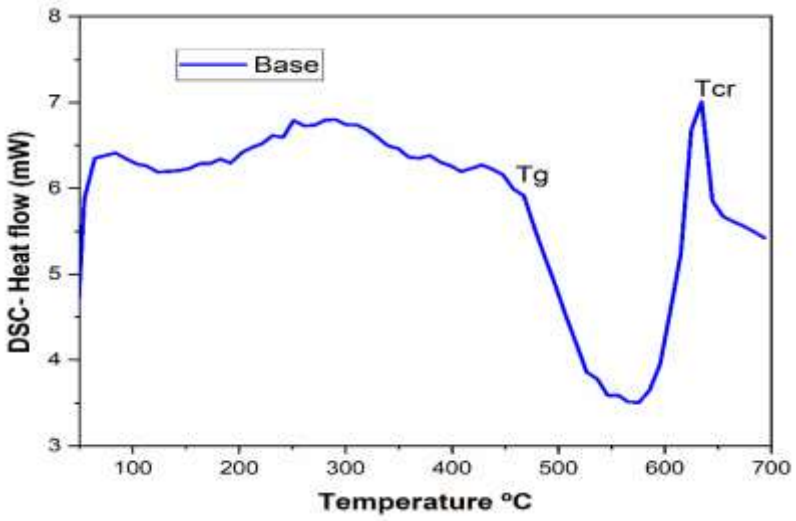

Figure 5.3 DSC graph of base 1393-B3 borate glass before sintering.

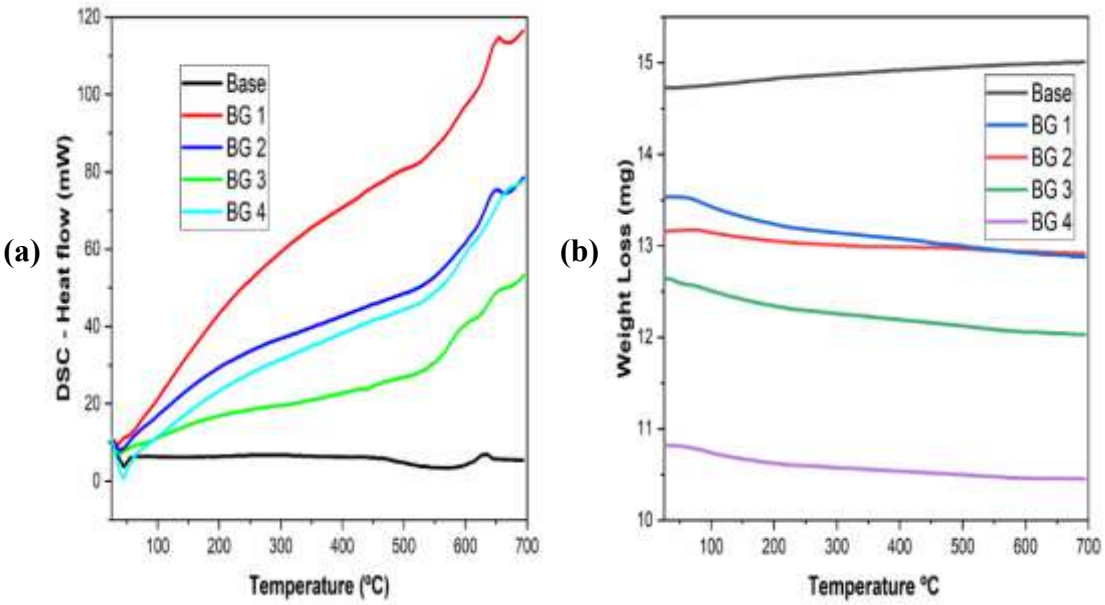

Figure 5.4 Thermal properties of base and TiO_2 substituted 1393-B3 glass samples **(a)** DSC graph and **(b)** TGA graph.

5.3.1.3 Thermal properties:

In Figure 5.3, the DSC study of base 1393-B3 borate glass sample exhibited a glass transition temperature of 467.5°C and glass crystallization temperature (Tcr) at 634.6°C. Figure 5.4a displays the DSC-heat flow graph for all the samples. This study showed that the substitution of boric oxide with TiO_2 resulted in a significant increase in heat flow, particularly at higher temperatures [52]. In comparison, TiO_2 has a very high melting temperature. The heat flow value decreases when a more significant proportion of TiO_2 is substituted. Figure 5.4a shows the glass transition temperature in the range of 450-520 ºC value, while the glass crystallization temperature is in the range of 600-700 ºC. Here, in Figure 5.4b, we obtained that the TGA weight loss value is altered very with a very small amount. We even observed that for base 1393-B3 borate glass, the weight loss value was increased at higher temperatures. For the TiO_2 substituted samples, the weight loss value starts decreasing in the temperature 30-70 ºC range. These results show better adaptability as weight loss decreased after TiO_2 substitution.

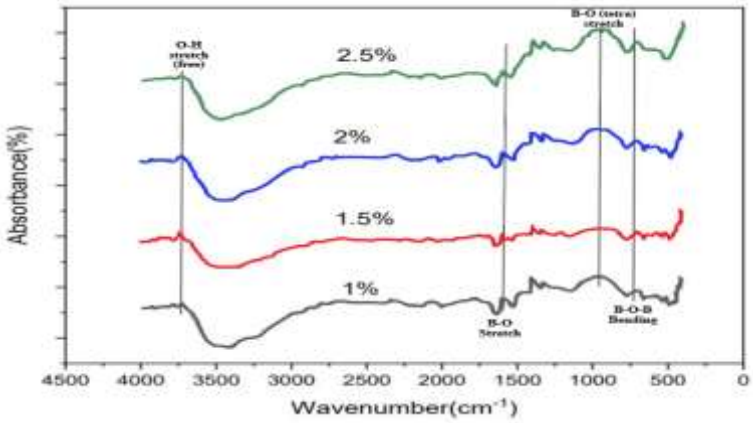

Figure 5.5 FTIR spectrum for different compositions of TiO_2 substituted 1393-B3 borate glass before immersion in SBF.

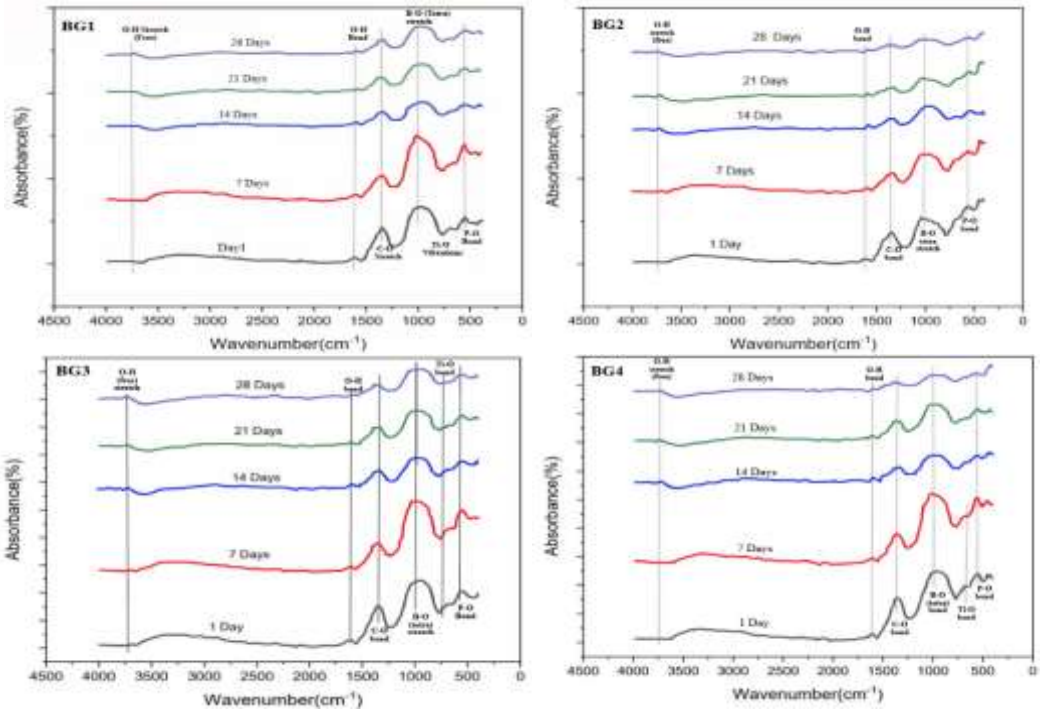

Figure 5.6 FTIR spectrum for BG1(1%), BG2(1.5%), BG3(2%) and BG4(2.5%) for different TiO_2 substituted 1393-B3 borate glass after 1,7,15,21 and 28 days immersion in SBF.

5.3.2 *In-vitro* analysis:

5.3.2.1 FTIR spectroscopy analysis:

FTIR absorbance spectra analysis was used to examine the presence of functional groups within the bioactive BG glass [53]. Figure 5.5 illustrates the bonding configuration observed in the different TiO_2 substituted samples. In this observation, the B-O bond stretch is

detected at a wavenumber of 740 cm-1, the B-O tetra bond stretch is seen at 975 cm-1, the B-O stretch is identified at 1580 cm-1, and the O-H bond stretch is found at 3690 cm-1. The presence of boron oxide and hydroxy linkages in the BG samples is shown. Figure 5.6 shows the various bonds present in 1% (BG1), 1.5% (BG2), 2% (BG3), and 2.5% (BG4) TiO_2 substituted 1393-B3 borate bioglass samples while submerged in SBF solution for different durations. In this study, we observed the stretching of B-O tetra bonds, hydroxyl bonds, and phosphate and carbonate bonds, which indicate the creation of an HA layer on the sample's surface [54].

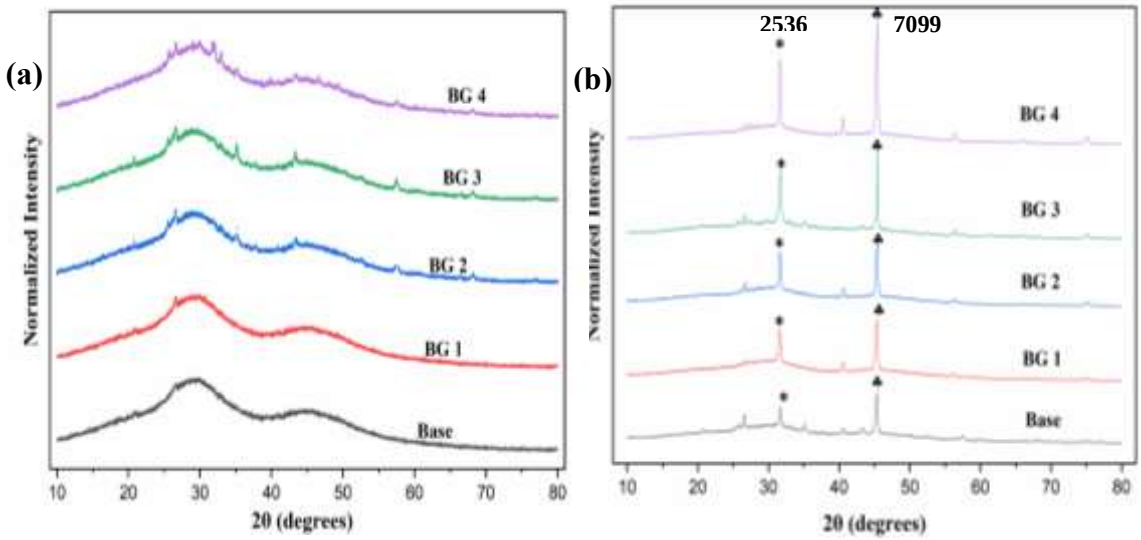

Figure 5.7 XRD graph of different wt % of TiO_2 substitution in 1393-B3 borate glass **(a)** before SBF immersion and **(b)** after SBF immersion.

5.3.2.2 XRD analysis:

The property of the obtained base and TiO_2 substituted 1393-B3 borate glass was found to be only amorphous in nature, and no indications of crystalline phase were seen either in the base glass or in the TiO_2 substituted 1393-B3 borate glass from the XRD pattern in (Figure 5.7a) proves that [52]. In this, we see that there is no sharp peak present in all five BG samples. In Figure 5.7b, we can observe a sharp peak at 31.6º (2 thetas) denoted with * denotes the creation of $Ca_{10.042}(PO_4)_{5.952}(OH)_{2.292}$ (JCPDS code-2536) HA bond in the 1393-B3 base and TiO_2 substituted 1393-B3 borate glass samples which were submerged in SBF solution for 28

days. So, the creation of the phosphate band occurs after 28 days. This steep peak indicates the creation of the HA link. Another steeper peak is also found at the base, and 1%, 1.5%, 2%, and 2.5% TiO_2 substituted 1393-B3 borate glass bioactive glasses. The steep peak at 45.3º (2 thetas) indicates the creation of a sodium phosphate bond, $Na_2(HPO)_4$ (code 7099), and this represents the phosphate bonds, as shown in JCPDS data analysis [54]. Thus, these findings suggest the creation of an HA layer on the surface, which leads to an increase in bioactivity.

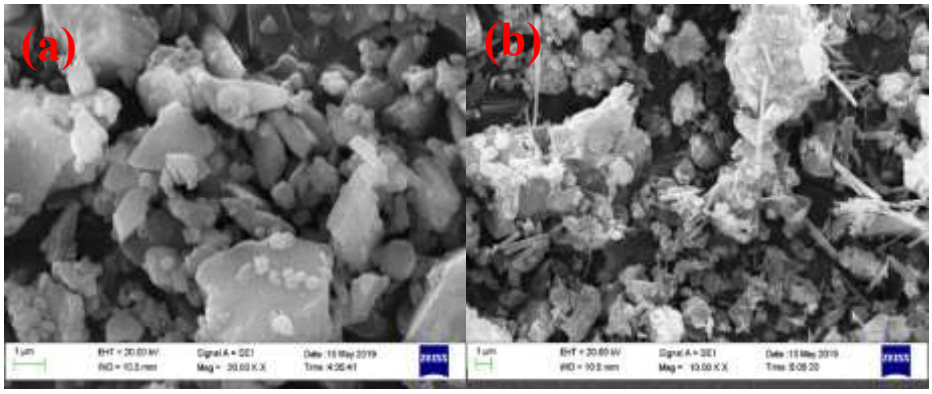

Figure 5.8.1 SEM image for base 1393-B3 borate bioactive glass sample **(a)** before SBF immersion and **(b)** after SBF immersion.

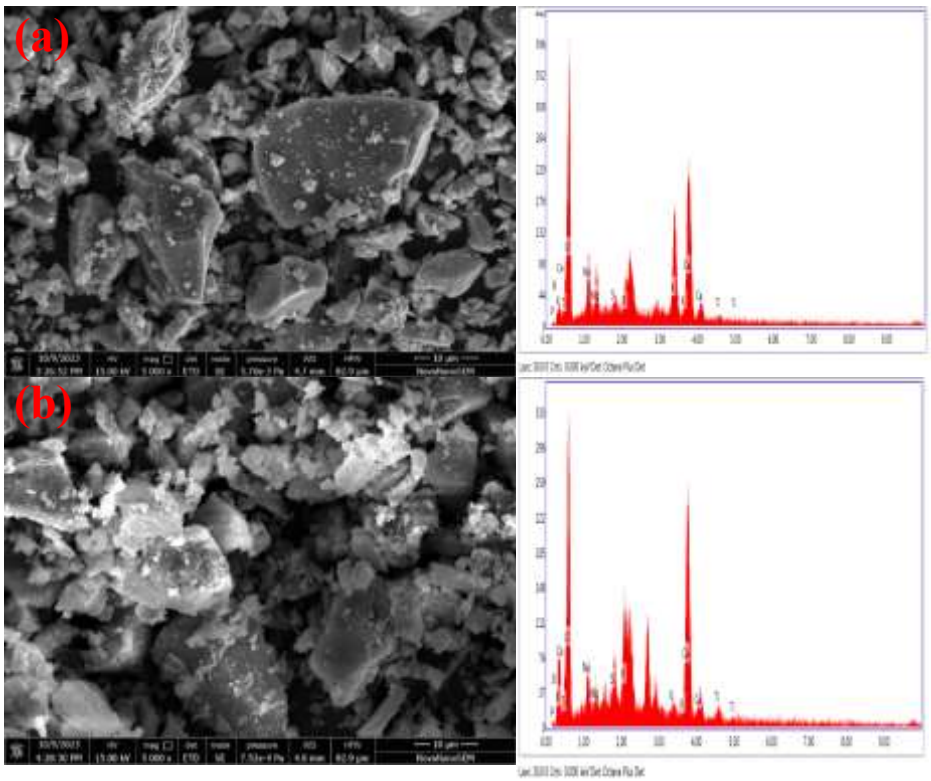

Figure 5.8.2 SEM-EDS image for 1 % TiO_2 substituted 1393-B3 borate bioactive glass sample **(a)** before SBF immersion and **(b)** after SBF immersion.

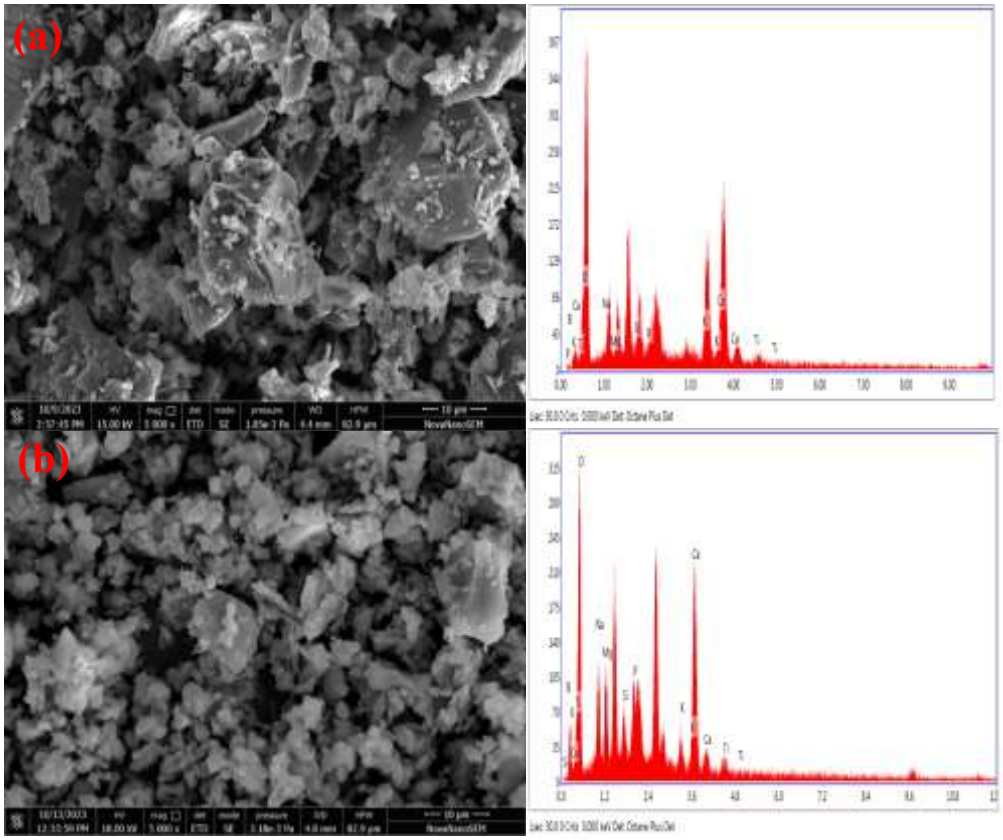

Figure 5.8.3 SEM-EDS image for 1.5 % TiO_2 substituted 1393-B3 borate bioactive glass sample **(a)** before SBF immersion and **(b)** after SBF immersion.

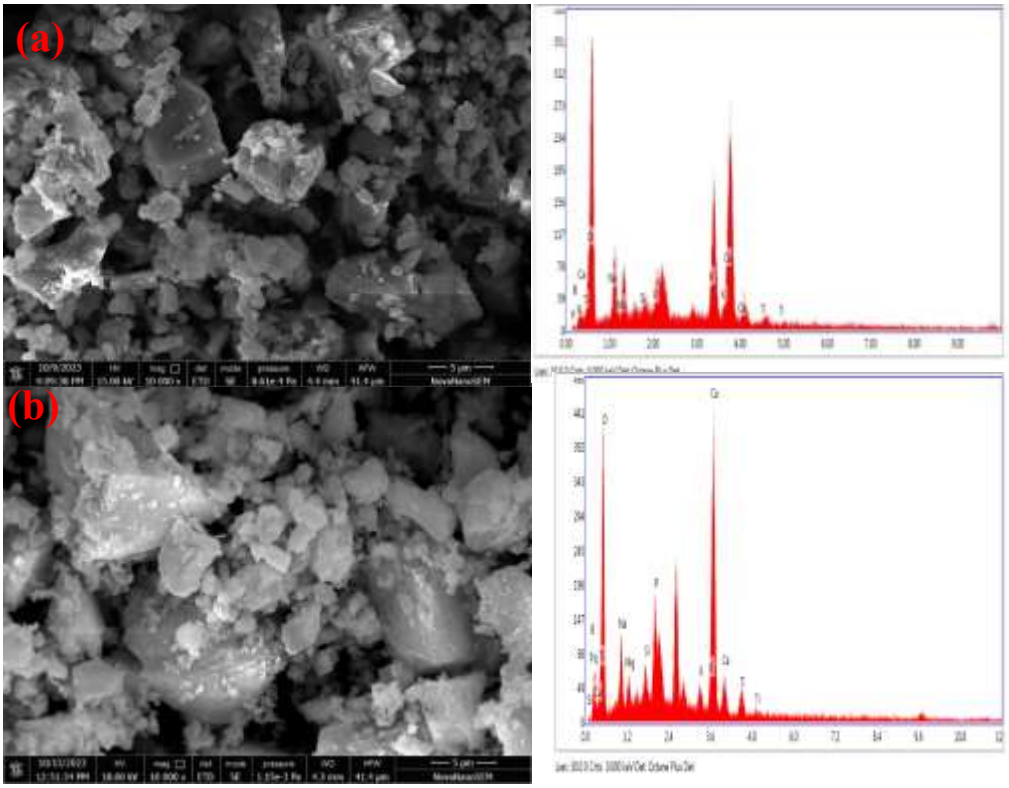

Figure 5.8.4 SEM-EDS image for 2 % TiO_2 substituted 1393-B3 borate bioactive glass sample **(a)** before SBF immersion and **(b)** after SBF immersion.

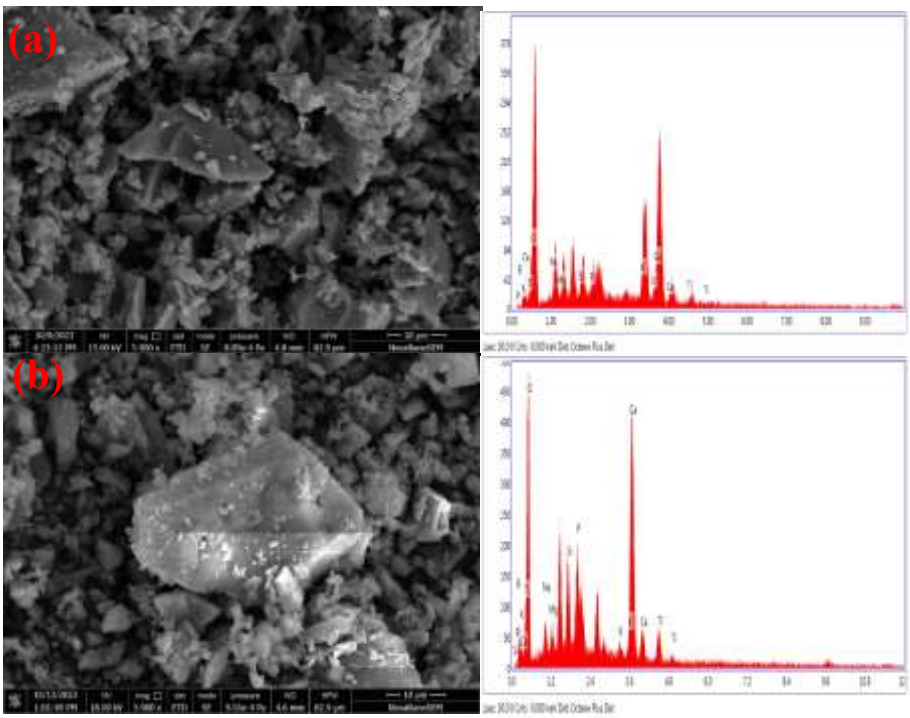

Figure 5.8.5 SEM-EDS image for 2.5 % TiO_2 substituted 1393-B3 borate bioactive glass sample **(a)** before SBF immersion and **(b)** after SBF immersion.

5.3.2.3 SEM-EDS analysis:

A SEM instrument is employed to examine the surface morphology of BG samples before and after immersion in SBF. EDS is used to identify the constituent components inside various samples. In Figure 5.8.1(a), it is clear that there are no layers in the base 1393-B3 borate sample. Conversely, figure 5.8.1(b) demonstrates the formation of a white spots layer, i.e., HA layer on the surface of the base 1393-B3 borate sample after immersion in SBF [41-45]. The SEM/EDAX images of 1%, 1.5%, 2%, and 2.5% (TiO_2 substituted) are shown in figures 5.8.2(a), 5.8.3(a), 5.8.4(a), and 5.8.5(a) correspondingly showing no layer on the surface, i.e. no elements of the HA layer. Figures 5.8.2(b), 5.8.3(b), 5.8.4(b), and 5.8.5(b) depict the SEM surface picture exhibiting a white HA layer on the samples. EDAX result displays the constituent components found within the samples. In the EDAX study, after SBF solution immersion, it was observed that the levels of phosphorus, calcium, and oxygen elements exhibited a rise, suggesting the creation of a HA layer.

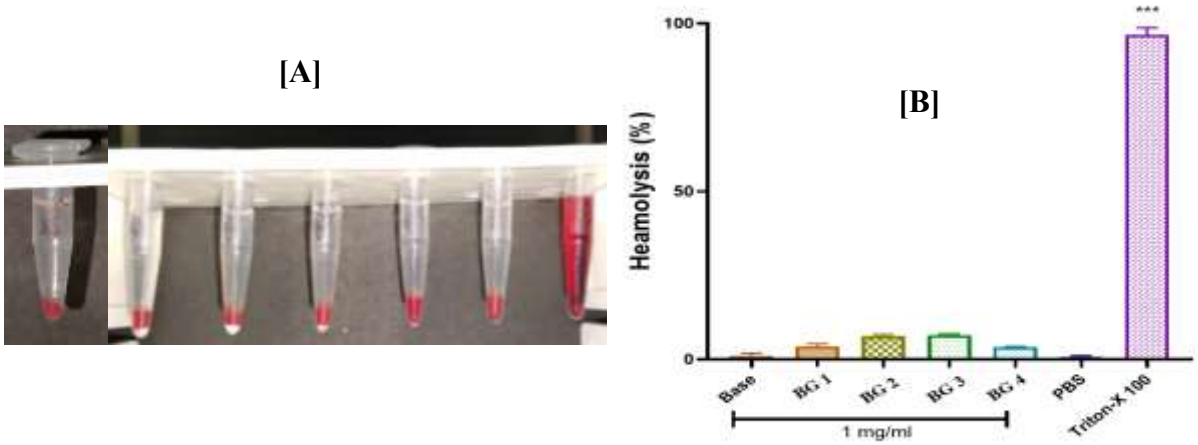

Figure 5.9 Ex vivo haemocompatibility of the TiO_2 substituted 1393-B3 borate glass **(A)** represents the after haemolytic study **(B)** % of haemolytic activity.

5.3.3 Hemocompatibility:

The experiment results indicated that all of the BG borate bioactive samples can be mixed with human blood. As shown in Figure 5.9(A), blood samples cannot be lysed. That's why we can say that it works with human blood [55]. As shown in Figure 5.9(B), the products caused less than 4% haemolysis, substantially lower ($p < 0.01$) than the positive control group (triton x-100), which was known to have a strong haemolytic effect [41]. The created items were found to be compatible with blood and would work for bone substitution.

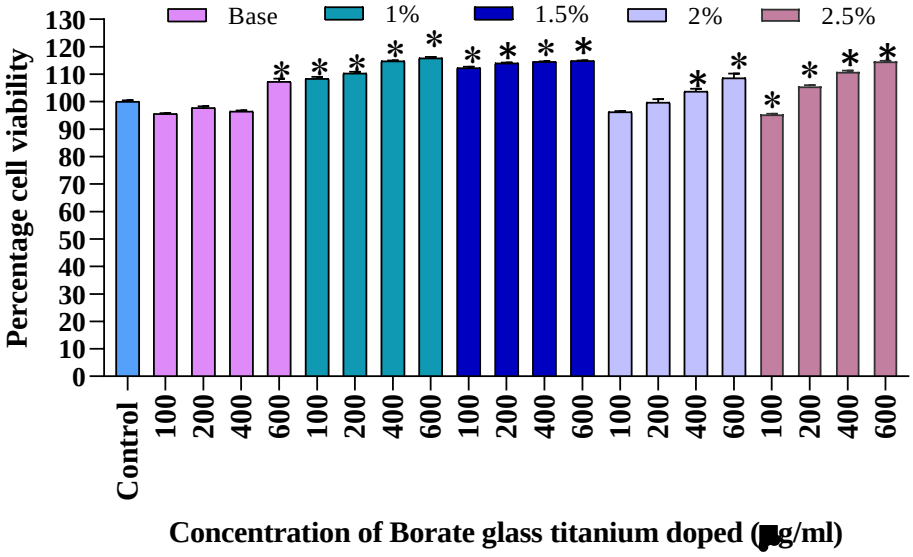

Figure 5.10.1 Bar diagram represents a cellular proliferation of titanium substituted with 1393-B3 borate glass sample against MG-63 cell line. Here * denotes a significant difference ($p<0.05$) compared to the control.

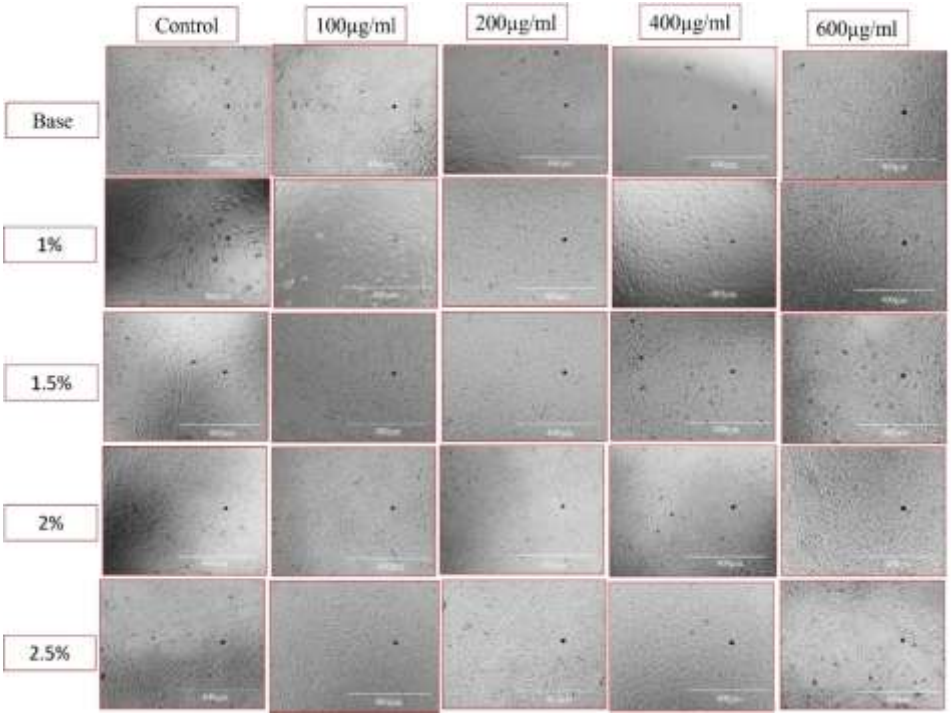

Figure 5.10.2 Phase contrast microscopic images (400µm) of TiO_2 substituted 1393-B3 glass samples (Base, 1%, 1.5%, 2%, and 2.5%) against MG-63 cell lines at various concentrations (100, 200,400 and 600µg/ml) showing proliferation of cells in a concentration-dependent manner.

5.3.4 *In-vitro* cellular analysis:

This study demonstrates the biocompatibility of all samples produced following the introduction of TiO_2 substitution, as seen by the bar graph and accompanying photos. The diagram illustrates a positive correlation between the proliferation value and the level of TiO_2 substitution in the BG borate bioactive samples.

5.3.4.1 Cellular compatibility assay:

The titanium-substituted 1393-B3 borate glass samples (Base, 1%, 1.5%, 2% and 2.5%) induced concentration-dependent proliferation against MG-63 cells even at higher concentrations. Significant proliferation was seen in the treatment group as compared to the control group. Thus, in Figure 5.10.1, the results suggested that titanium borate glass samples significantly support cell survival and growth, which signifies a potential scope for bone regeneration [55].

5.3.4.2 Phase-contrast Imaging:

In-vitro cell imaging with phase contrast microscope data revealed that the proliferation of MG-63 cells increased with the concentration of titanium in 1393-B3 borate glass samples. As shown in Figure 5.10.2, Cells were proliferated maximally in 1% titanium-substituted 1393-B3 borate glass samples at the concentration of 600 µg/ml. This further validates the result of the cellular compatibility assay. Thus, the present result demonstrates that titanium substituted 1393-B3 borate glass samples have a significant application on bone regeneration.

5.4 Summary

Based on the observed data, it can be concluded that the 1393-B3 borate bioactive glass substituted with TiO_2 exhibits different bioactivity. Earlier XRD had an amorphous character, with no evidence of a crystalline phase detected in the base glass or either in the TiO_2-substituted borate glass. The bioactivity of bioglass samples was shown by the use of SBF and subsequent testing utilizing XRD, FTIR, and SEM/EDAX characterizations. The identification of HA within the obtained data indicates the existence of bioactivity in the bioactive glass materials. It has been observed that different TiO_2 substitution percentages have a considerable impact on the mechanical properties of the samples, particularly those associated with bone replacement. Haemocompatibility results show that they are compatible with human blood. During an investigation of cellular compatibility on the MG-63 osteosarcoma cell line, it was shown that introducing TiO_2 into 1393-B3 borate bioactive glass samples resulted in an enhancement of cell proliferation. The best result for cellular compatibility is found for 1% TiO_2 substituted 1393-B3 borate bioactive glass. The findings indicate that the incorporation of TiO_2 into the 1393-B3 borate bioactive glass enhances its bioactivity, making it a potentially suitable substitute for orthopaedic implants used in joint replacement surgeries.

References:

[1] L.L. Hench, The story of Bioglass, J Mater Sci Mater Med. 17 (2006) 967–978.

[2] L.L. Hench, Bioactive materials: The potential for tissue regeneration, J. Biomed. Mater. Res. 21 (1998) 511–518.

[3] L.L. Hench, R.J. Splinter, W.C. Allen, Bonding Mechanisms at the Interface of Ceramic Prosthetic Materials, I. Biomed. Mater. Res. Symp. 2 (1971) 117–141.

[4] L. Hench, J. Polak, Third-Generation Biomedical Materials, Body Building: The B Ion. Hum. 295 (2002) 1014–1017.

[5] D. Shekhawat, A. Singh, M.K. Banerjee, T. Singh, A. Patnaik, Bioceramic composites for orthopaedic applications: A comprehensive review of mechanical, biological, and microstructural properties, Ceramics International 47 (2021) 3013–3030.

[6] L.L. Hench, N. Roki, M.B. Fenn, Bioactive glasses : Importance of structure and properties in bone regeneration, J. Mol. Struct. 1073 (2014) 24–30.

[7] L.L. Hench, J.R. Jones, Bioactive Glasses: Frontiers and Challenges, Frontiers in Bioengineering and Biotechnology 3 (2015) 1–12.

[8] T. Kokubo, H. Kushitani, S. Sakka, T. Kitsugi, T. Yamamuro, Solutions able to reproduce in vivo surface-structure changes in bioactive glass-ceramic A-W3, Journal of Biomedical Materials Research 24 (1990) 721–734.

[9] T. Kokubo, H. Takadama, How useful is SBF in predicting in vivo bone bioactivity?, Biomaterials 27 (2006) 2907–2915.

[10] V. Salih, K. Franks, M. James, G.W. Hastings, J.C. Knowles, I. Olsen, Development of soluble glasses for biomedical use Part II : The biological response of human osteoblast cell lines to phosphate-based soluble glasses, J. Mater. Sci. Mater. Med. II. 1 (2000) 615–620.

[11] P. Ducheyne, Q. Qiu, Bioactive ceramics: the effect of surface reactivity on bone formation and bone cell function, Biomaterials 20 (1999), 2287–2303.

[12] N. Price, S. P. Bendall, C. Frondoza, R. H. Jinnah, D. S. Hungerford, Human osteoblast-like cells (MG63) proliferate on a bioactive glass surface, Journal of Biomedical Materials Research 37 (1997) 394–400.

[13] V. Kandi, S. Vadakedath, Implant-Associated Infections: A Review of the Safety of Cardiac Implants, Cureus 12 (2020) 12 e12267.

[14] J.R. Lentino, Prosthetic joint infections: bone of orthopedists, challenge for infectious disease specialists, Clin. Infect. Dis. 36 (2003) 1157–1161.

[15] I. Qayoom, A.K. Teotia, A. Panjla, S. Verma, A. Kumar, Local and sustained delivery of rifampicin from a bioactive ceramic carrier treats bone infection in rat tibia, ACS Infect. Dis. 13 (2020) 2938–2949.

[16] R. A. Youness, M.S. Amer, M. A. Taha, Comprehensive In Vivo and In Vitro Studies for Evaluating the Bone-Bonding Ability of Na2O–CaO–SiO2–B2O3–Ag2O Glasses for Fracture Healing Applications. Journal of Inorganic and Organometallic Polymers and Materials 33 (2023) 4068–4082.

[17] R.A. Youness, E. Al-Ashkar, M. A. Taha, Role of porosity in the strength, dielectric properties, and bioactivity of hardystonite ceramic material for use in bone tissue engineering applications. Ceramics International 49 (2023) 40520–40531.

[18] W.S. Abushanab, E.B. Moustafa, R.A. Youness, Mechanical behavior and tribological properties of hydroxyapatite/hardystonite/zirconia hybrid nanocomposites for orthopedic applications. Applied Physics A 129 (2023) 394.

[19] A.M. Alturki, A.S. Alatawi, D.E. Abulyazied, H.M. Abomostafa, G.M. el komy, R. Alamlah, M.A. Taha, R.A. Youness, Magnetic and Dielectric Properties of Hybrid Nanocomposites of Biologically Extracted Hydroxyapatite/Hematite/Silicon Dioxide for

Potential Use in Bone Replacement Applications. ECS Journal of Solid State Science and Technology 12 (2023) 083001.

[20] A.B. Khoshaim, E.B. Moustafa, R.A. Youness, Antibacterial, mechanical, and dielectric properties of hydroxyapatite cordierite/zirconia porous nanocomposites for use in bone tissue engineering applications. Nanotechnology Reviews, 13 (2024) : 20230175.

[21] R.A. Youness, M.A. Taha, Tuning biodegradability, bone-bonding capacity, and wear resistance of zinc-30% magnesium intermetallic alloy for use in load-bearing bone applications. Scientific Reports, 14 (2024) 1-22.

[22] M.A. Ur Rehman, F.E. Bastan, A. Nawaz, Q. Nawaz, A. Wadood, Electrophoretic deposition of PEEK/bioactive glass composite coatings on stainless steel for orthopedic applications: an optimization for in vitro bioactivity and adhesion strength, The International Journal of Advanced Manufacturing Technology, 108 (2020) 1849–1862.

[23] A. Ewald, S.K. Glückermann, R. Thull, U. Gbureck, Antimicrobial titanium/silver PVD coatings on titanium, Biomed. Eng. Online 5 (2006) 22.

[24] N. Drnovšek, K. Rade, R. Milačič, J. Štrancar, S. Novak, The properties of bioactive TiO2 coatings on Ti-based implants. Surface and Coatings Technology, 209 (2012). 177–183.

[25] V.A. Ponomarev, A.D. Popova, A.N. Sheveyko, E.S. Permyakova, K.A. Kuptsov, A.S. Ilnitskaya, P.V. Slukin, S.G. Ignatov, N.A. Gloushankova, B. Subramanian, D.V. Shtansky, Microstructure and biological properties of titanium dioxide coatings doped with bioactive and bactericidal elements, Applied Surface Science 575 (2022) 151755.

[26] T. Kokubo, T. Matsushita, H. Takadama, Titania-based bioactive materials. Journal of the European Ceramic Society 27 (2007) 1553–1558.

[27] M. Bavanilatha, L. Yoshitha, S. Nivedhitha, S. Sahithya, Bioactive studies of TiO2 nanoparticles synthesized using Glycyrrhiza glabra, Biocatalysis and Agricultural Biotechnology 19 (2019) 101131.

[28] R. Samudrala, V. Penugurti, B. Manavathi, Cytocompatibility studies of titania-doped calcium borosilicate bioactive glasses in-vitro, Materials Science and Engineering: C 77 (2017) 772–779.

[29] L. Liu, R. Bhatia, T. Webster, Atomic layer deposition of nano-TiO_2 thin films with enhanced biocompatibility and antimicrobial activity for orthopedic implants, International Journal of Nanomedicine 12 (2017) 8711–8723.

[30] S. Noreen, E. Wang, H. Feng, Z. Li, Functionalization of TiO2 for Better Performance as Orthopedic Implants, Materials 15 (2022) 6868.

[31] W.G. Woods, An introduction to boron: history, sources, uses, and chemistry, Environmental Health Perspectives 102 (1994) 5–11.

[32] M. Bengisu, Borate glasses for scientific and industrial applications: a review, Journal of Materials Science 51 (2016) 2199–2242.

[33] A.A. Aslam, J. Akram, R.A. Mehmood, A. Mubarak, A. Khatoon, U. Akbar, S.A. Ahmad, M. Atif, Boron-based bioactive glasses: Properties, processing, characterization and applications, Ceramics International 49 (2023) 19595–19605.

[34] R.F. Barth, A.H. Soloway, R.G. Fairchild, Boron Neutron Capture Therapy for Cancer, Scientific American 263 (1990) 100–107.

[35] A.R. Ghazy, B.M. Elmowafy, A.M. Abdelghany, T.M. Meaz, R. Ghazy, R.M. Ramadan, Structural, optical, and cytotoxicity studies of laser irradiated ZnO doped borate bioactive glasses, Scientific Reports 13 (2023) 7292.

[36] M.A. Marzouk, F. H.ElBatal, H.A. ElBatal, Effect of TiO2 on the optical, structural and crystallization behavior of barium borate glasses, Optical Materials 57 (2016) 14–22.

[37] A.H. Hammad, A.M. Abdelghany, H.A. Elbatal, The influence of titanium ions on crystallization, morphological, and structural properties of strontium borate glass, Journal of Non-Crystalline Solids 450 (2016). 66–74.

[38] S.K. Singh, J. Kumar, P. Singh, S.K. Rajput, A. K. Dubey, R Pyare, P.K. Roy, Impact of 13-93 Bio-glass Inclusion on the Machinability, In-vitro Degradation, and Biological Behavior of Y-TZP-based Bioceramic Composite, Ceramics International 50 (2024) 1087-1106.

[39] A. Ali, M. Ershad, V. K. Vyas, S. K. Hira, P. P. Manna, B. N. Singh, S. Yadav, P. Srivastava, S. P. Singh, R. Pyare, Studies on effect of CuO addition on mechanical properties and in vitro cytocompatibility in 1393 bioactive glass scaffold, Materials Science and Engineering: C 93 (2018) 341–355.

[40] A. Ali, S. P. Singh, R. Pyare, SrO assisted 1393 glass scaffold with enhanced biological compatibility, Journal of Non-Crystalline Solids 550 (2020) 120392.

[41] S.K. Yadav, S. Ray, M. Ershad, V.K. Vyas, S. Prasad, A. Ali, S. Yadav, M.R. Majhi, R. Pyare, Development of Zirconia Substituted 1393 Bioactive Glass for Orthopaedic Application, Oriental Journal of Chemistry 33 (2017) 2720–2730.

[42] S. Yadav, P. Singh, R. Pyare, Synthesis, characterization, mechanical and biological properties of biocomposite based on zirconia containing 1393 bioactive glass with hydroxyapatite, Ceramics International 46 (2020) 10442–10451.

[43] S.K. Yadav, V. K. Vyas, S. Prasad, R. Pyare, FABRICATION AND ANALYSIS OF THE EFFECT OF DOPING TIO2 IN 1393 BIOACTIVE GLASS, International Journal of Advanced Research 4 (2016) 891–900.

[44] G.J. Mohini, G.S. Baskaran, V.R. Kumar, M. Piasecki, N. Veeraiah, Bioactivity studies on TiO2-bearing Na2O–CaO–SiO2–B2O3 glasses. Materials Science and Engineering: C 57 (2015) 240–248.

[45] G.J. Mohini, N. Krishnamacharyulu, G. Sahaya Baskaran, P. V. Rao, N. Veeraiah, Studies on influence of aluminium ions on the bioactivity of B2O3–SiO2–P2O5–Na2O–CaO glass system by means of spectroscopic studies. Applied Surface Science 287 (2013) 46–53.

[46] N. Mutlu, F. Kurtuldu, I. Unalan, Z. Neščáková, H. Kaňková, D. Galusková, M. Michálek, L. Liverani, D. Galusek, A. R. Boccaccini, Effect of Zn and Ga doping on bioactivity, degradation, and antibacterial properties of borate 1393-B3 bioactive glass, Ceramics International 48 (2022) 16404–16417.

[47] B. Elmowafy, A. Abdelghany, R. Ramadan, R. Ghazy, T. Meaz, Synthesis, structural characterization, and antibacterial studies of new borate 13-93B3 bioglasses with low copper dopant, Egyptian Journal of Chemistry 65 (2022) 1–10.

[48] C. Pramanik, T. Wang, S. Ghoshal, L. Niu, B.A. Newcom, Y. Liu, C.M. Primus, H. Feng, D.H. Pashley, S. Kumara, F.R. Tay, Interaction of microfibrous borate bioactive glass dressing with bone-bound bisphosphonate in the presence of simulated body fluid, J. Mater. Chem. B 3 (2015) 959–963.

[49] S.S. Hossain, S. Yadav, S. Majumdar, S. Krishnamurthy, R. Pyare, P.K. Roy, A comparative study of physico-mechanical, bioactivity, and hemolysis properties of pseudo-wollastonite and wollastonite glass-ceramic synthesized from solid wastes, Ceram. Int. 46 (2020) 833–843.

[50] C. Liao, F. Lin, K. Chen, J. Sun, Thermal decomposition and reconstitution of hydroxyapatite in air atmosphere, Biomaterials 20 (1999) 1807–1813.

[51] A. Najafinezhad, M. Abdellahi, H. Ghayour, A. Soheily, A. Chami, A. Khandan, A comparative study on the synthesis mechanism, bioactivity, and mechanical properties of three silicate bioceramics, Mater. Sci. Eng. C 72 (2017) 259–267.

[52] U. Kumar, D. Yadav, A. K. Thakur, K. K. Srivastav, S. Upadhyay, Investigation on phase formation of Sr2SnO4 and effect of La-doping on its structural and optical properties, Journal of Thermal Analysis and Calorimetry 135 (2019) 1987–1999.

[53] J. Xia, Y. Xiong, S. Min, J. Li, A review of recent infrared spectroscopy research for paper, Applied Spectroscopy Reviews 58 (2022) 738-754.

[54] A. Singh, P. Goswami, B. Koch, P. Singh, R. Pyare, Study of Human Osteosarcoma Cell Line Growth, Hemocompatibility, In-vitro Analysis and Physical Properties of V_2O_5 Substituted Borosilicate Glass, Silicon (2024) 1876-9918

[55] V. Kushwah, S.S. Katiyar, C.P. Dora, A.K. Agrawal, D.A. Lamprou, R.C. Gupta, S. Jain, Co-delivery of docetaxel and gemcitabine by anacardic acid modified self-assembled albumin nanoparticles for effective breast cancer management, Acta Biomaterialia 73 (2018) 424–436.